INTERNATIONAL JOURNAL OF ROBUST AND NONLINEAR CONTROL
Int. J. Robust. Nonlinear Control 2012; **22**:2055–2083
Published online 29 September 2011 in Wiley Online Library (wileyonlinelibrary.com). DOI: 10.1002/rnc.1808

Optimization of airborne wind energy generators

Lorenzo Fagiano[1,2], Mario Milanese[3,*,†] and Dario Piga[1]

[1]*Dipartimento di Automatica e Informatica, Politecnico di Torino, Torino, Italy*
[2]*Department of Mechanical Engineering, University of California Santa Barbara, Santa Barbara, CA, USA*
[3]*Kitenergy S.r.l., Torino, Italy*

SUMMARY

This paper presents novel results related to an innovative airborne wind energy technology, named Kitenergy, for the conversion of high-altitude wind energy into electricity. The research activities carried out in the last five years, including theoretical analyses, numerical simulations, and experimental tests, indicate that Kitenergy could bring forth a revolution in wind energy generation, providing renewable energy in large quantities at a lower cost than fossil energy. This work investigates three important theoretical aspects: the evaluation of the performance achieved by the employed control law, the optimization of the generator operating cycle, and the possibility to generate continuously a constant and maximal power output. These issues are tackled through the combined use of modeling, control, and optimization methods that result to be key technologies for a significant breakthrough in renewable energy generation. Copyright © 2011 John Wiley & Sons, Ltd.

Received 17 February 2011; Revised 28 July 2011; Accepted 5 August 2011

KEY WORDS: wind energy; high-altitude wind energy; nonlinear model predictive control; optimization

1. INTRODUCTION

Wind industry has the largest share of renewable energy generation, apart from hydropower, with a yearly global growth of the installed capacity of about 30% in the last years [1]. Indeed, by exploiting 20% only of the world land sites that are profitable for the actual wind technology, based on wind towers, in principle, the global energy demand could be supplied [2]. However, the current wind technology has limitations in terms of energy production costs, which are still too high with respect to fossil sources, and in terms of land occupation, because wind farms based on modern wind towers with 2- to 3-MW rated power have an average power density of 3.5–4 MW/km^2 [3], about 200–300 times lower than that of large thermal plants. A comprehensive overview of the present wind technology is given in [4], where it is also pointed out that no breakthrough is expected, but many evolutionary steps that can cumulatively bring up to 30%–40% improvements of cost-effectiveness over the next decades. In fact, wind turbines already operate at a height of about 150 m over the ground, a value hardly improvable, because of structural constraints that give rise to technological and economical limits. Yet the wind speed generally increases with the height above the ground: for example, at the height of 500–1000 m, the mean wind power density is about four times the one at 50–150 m and 40 times the one at 10,000 m [5]. This point suggests that a breakthrough in wind energy generation can be realized by capturing wind power at altitudes over the ground that cannot be reached by wind towers. The idea of harnessing high-altitude wind power using a tethered aircraft has been proposed at least as far back as the 1970s [6–8]. However, only in the past few years, more intensive theoretical, technological, and experimental studies have been carried out

*Correspondence to: Mario Milanese, Modelway S.r.l., Torino, Italy.
†E-mail: mario.milanese@kitenergy.net

by academic research groups and/or high-tech companies, and several technologies have been proposed and investigated in order to harness the power of high-altitude wind (see, e.g., [9–20]). These approaches, indicated as airborne wind energy (AWE) technologies, involve a large spectrum of different features and technical solutions, whose detailed presentation is not possible in this paper. It has to be noted that AWE technologies are being investigated also for naval propulsion (see, e.g., [21, 22]) and for offshore electric energy generation [23].

Since 2005 at Politecnico di Torino, an AWE technology, indicated here as Kitenergy, has been extensively investigated through modeling, computer simulation, and experimental verification on a prototype [10–12]. The main conclusion emerging from these studies is that Kitenergy technology has the potential to achieve energy generation costs that are lower than those of fossil energy and an amount of yearly generated energy per unit area of occupied land that is 5–15 times higher than that of the present wind technology. Thus, Kitenergy technology may represent a quantum leap in overcoming two main limitations of the present wind technology. These results can be obtained mainly thanks to the fact that energy is generated at the ground level and that the tethered wing flies in 'crosswind' conditions [8], thus generating large aerodynamical lift forces, which are exploited to produce mechanical power. Indeed, other technical aspects related to the operational safety and reliability of these generators, as well as to the issues of energy storage and grid connection, will also need to be addressed in the near future. However, the authors think that solutions to these problems can be obtained without reducing the potentials of the concept, in terms of quantity of generated energy, cost, and land occupation. For example, the problem of potential damage due to line failure has been considered in the design of Kitenergy technology, which makes use of two lines, differently from most of other AWE technologies that employ one line. If one of the two lines breaks, the wing loses most of its aerodynamic forces and can be easily recovered with the remaining line. Regarding the interaction with low-flying aircrafts, a farm with many Kitenergy generators should have a no-fly zone around it, as it is, at present, required for nuclear plants. According to our studies, in a good site, the no-fly zone required to generate, on average, 1 GW of power per year from high-altitude winds would be smaller than the no-fly zones that are actually issued around nuclear plants with the same rated power.

In this paper, the main modeling and control techniques of Kitenergy technology are outlined, and new results are presented on two configurations for energy generation, indicated as KE-yoyo and KE-carousel configurations. This paper is organized as follows. Section 2 is devoted to the description of the concepts of Kitenergy technology, of the related modeling and control aspects, and of the problems treated in this paper. Such problems are dealt with by the new results provided in Section 3 and illustrated through numerical simulations in Section 4. Finally, conclusions are given in Section 5.

2. KITENERGY TECHNOLOGY AND PROBLEM DESCRIPTION

2.1. Technology concept

The concept of Kitenergy is to use wings, linked to the ground by two cables, to extract energy from wind blowing at higher heights with respect to those of the actual wind technology. The flight of the wings is suitably driven by an automatic control unit. Wind energy is collected at ground level by converting the traction forces acting on the wing lines into electrical power with the use of suitable rotating mechanisms and electric generators placed on the ground. The wings are able to exploit wind flows at higher altitudes than those of wind towers (up to 1000 m, using 1200- to 1500-m-long cables), where stronger and more constant wind can be found basically everywhere in the world. In this way, high-altitude wind energy can be harvested with the minimal effort in terms of generator structure, cost, and land occupation. In the actual wind towers, the outermost 30% of the blade surface approximately contributes for 80% of the generated power. The main reason is that the effective wind speed on the blade is higher in the outer part, and wind power grows with the cube of the effective wind speed. Yet, the structure of a wind tower determines most of its cost and imposes a limit to the elevation that can be reached. To understand the concept of Kitenergy, one can imagine to remove all the bulky structure of a wind tower and just keep the outer part of the blades,

DOI: 10.1002/rnc

which becomes a much lighter wing flying fast in crosswind conditions (Figure 1), connected to the ground by the cables. Thus, the rotor and the tower of the present wind technology are replaced in Kitenergy technology by the wing and its cables, realizing a wind generator that is largely lighter and cheaper. For example, in a 2-MW wind turbine, the weight of the rotor and the tower is typically about 300 tons [24]. A Kitenergy generator of the same rated power can be obtained using a 500-m^2-size wing and 1000-m-long cables, with a total weight of about 2–3 tons only.

2.2. *Kitenergy configurations and operating cycles*

At ground level, the two wing cables are rolled around winches, linked to electric drives that are able to act either as generators or as motors. The kite flight is tracked using onboard wireless instrumentation (GPS and magnetic and inertial sensors) as well as ground sensors to measure the wing speed and position, the power output, the cable force and speed, and the wind speed and direction. Such variables are employed for feedback control by a control system, able to influence the kite flight by differentially pulling the cables via a suitable action of the electric drives. The system composed of the electric drives, the drums, the onboard sensors, and all the hardware needed to control a single kite is denoted as Kite Steering Unit (KSU), and it is the core of the Kitenergy technology (Figure 2). The KSU can be employed in different ways to generate energy, depending on how the traction forces acting on the cables are converted into mechanical and electrical power. In particular, two different configurations have been investigated so far, namely the KE-yoyo and the KE-carousel configurations.

KE-yoyo configuration. In the KE-yoyo configuration, the KSU is fixed with respect to the ground. Energy is obtained by continuously performing a two-phase cycle (depicted in Figure 3). In the *traction phase*, the controller is designed in such a way that the kite unrolls the lines, maximizing the power generated by the electric drives that are driven by the rotation of the drums. When the maximum line length is reached, the *passive phase* begins, and the drives act as motors, spending a

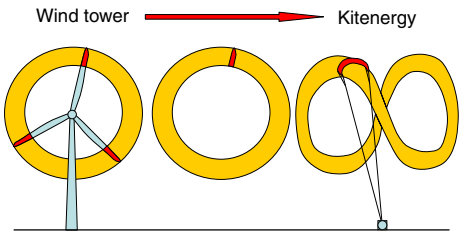

Figure 1. Concept of Kitenergy technology.

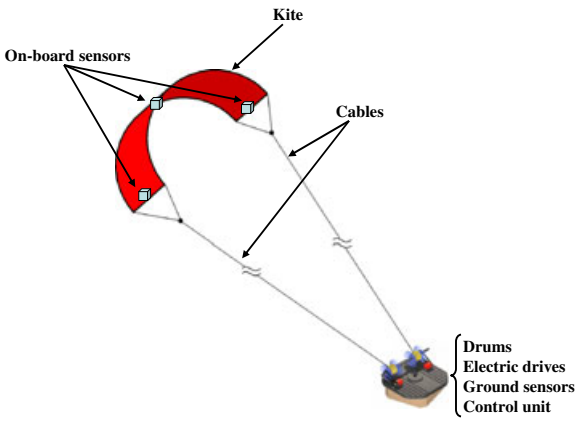

Figure 2. Scheme of a Kite Steering Unit.

DOI: 10.1002/rnc

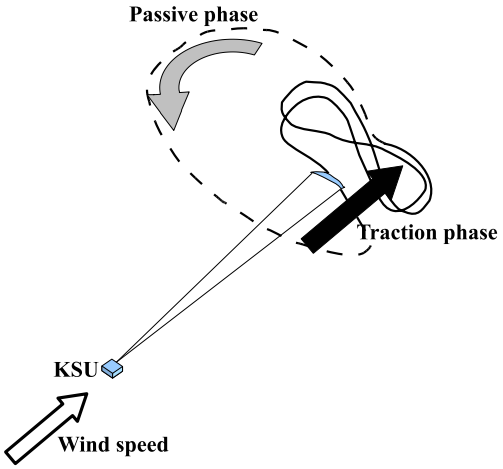

Figure 3. Sketch of a KE-yoyo cycle: traction (solid) and passive (dashed) phases. KSU, Kite Steering Unit.

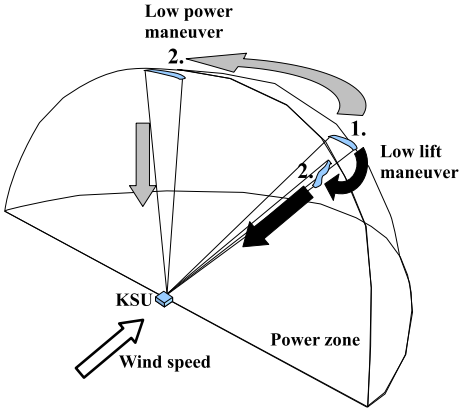

Figure 4. KE-yoyo passive phase: 'low-power' (gray) and 'low-lift' (black) maneuvers. KSU, Kite Steering Unit.

minimum amount of the previously generated energy to recover the kite and to drive it in a position that is suitable to start another traction phase. The passive phase can be performed in two possible ways (Figure 4).

(i) **Low-power maneuver**. The kite is driven to the borders of the 'power zone', where the effective wind speed (and, consequently, the aerodynamic lift force) drops to low values, thus allowing the cables to recover with low energy expense.
(ii) **Low-lift maneuver**. With the use of additional actuators onboard the wing, the attack angle is modified in order to make the kite reduce its aerodynamic lift and to allow a fast winding back of the cables with low energy losses.

The low-lift maneuver has the advantage of occupying less aerial space than the low-power maneuver; however, it requires additional actuators on the kite. For the whole KE-yoyo cycle to be generative, the total amount of energy produced in the traction phase has to be greater than the energy spent in the passive one. The controller employed in the traction phase must maximize the produced energy, whereas in the passive phase, the objective is to maneuver the kite in a suitable way to minimize, at the same time, the spent energy (see, e.g., [11, 25] for details).

KE-carousel configuration. In a KE-carousel, the KSU is placed on a vehicle moving along a circular path (Figure 5); the vehicle wheels are connected to electric drives, which can generate

DOI: 10.1002/rnc

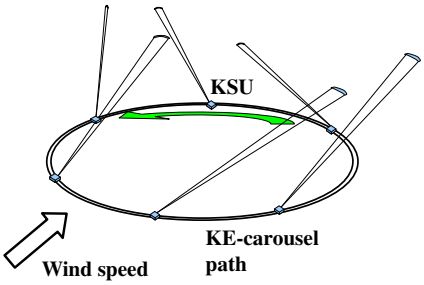

Figure 5. Sketch of a KE-carousel. KSU, Kite Steering Unit.

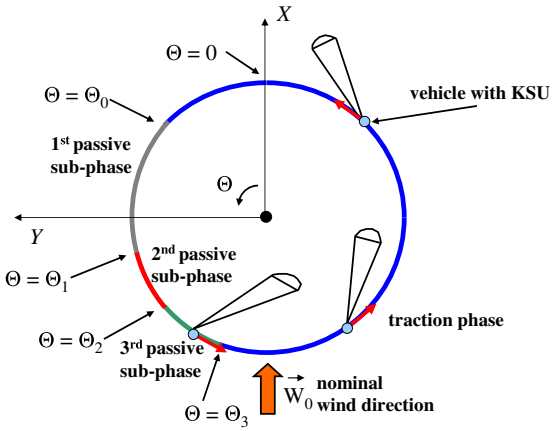

Figure 6. KE-carousel configuration phases with constant line length. KSU, Kite Steering Unit.

electric energy. The drives are suitably controlled in order to also regulate the vehicle speed. The potentials of the KE-carousel configuration have been investigated using either variable line length or constant line length.

(i) **Constant line length**. When a fixed cable length is employed, energy is generated by continuously repeating a cycle composed of two phases, namely the *traction* and the *passive* phases. These phases are related to the angular position Θ of the control unit, with respect to the wind direction (Figure 6). During the traction phase, which begins at $\Theta = \Theta_3$ in Figure 6, the controller is designed in such a way that the kite pulls the vehicle, maximizing the generated power. This phase ends at $\Theta = \Theta_0$ when the passive phase begins: the kite is no more able to generate energy until angle Θ reaches the value Θ_3. In the passive phase, the controller is designed to move the kite, with the minimal energy loss, in a suitable position to begin another traction phase, where, once again, the control algorithm is designed to maximize the generated power. According to the control strategy of the constant-line carousel, the passive phase is divided into three subphases, delimited by the angular positions Θ_1 and Θ_2 in Figure 6 (see, e.g., [10, 25] for details).

(ii) **Variable line length**. If line rolling/unrolling is suitably managed during the cycle, energy can be generated also when the vehicle is moving against the wind. In this case, the operating phases, namely the *traction* and the *unroll* phases, are depicted in Figure 7. The *unroll phase* approximately begins when the angular position Θ of the vehicle is such that the KSU is moving in the opposite direction with respect to the nominal wind: such situation is identified by angle Θ_0 in Figure 7. During the unroll phase, the electric drives linked to the vehicle wheels act as motors to drag the KSU against the wind. At the same time, the kite lines unroll; thus, energy is generated as in the traction phase of the KE-yoyo configuration. The difference between the energy spent to drag the vehicle and the energy generated by unrolling the lines gives the net energy generated during this phase. When the KSU starts moving with wind

DOI: 10.1002/rnc

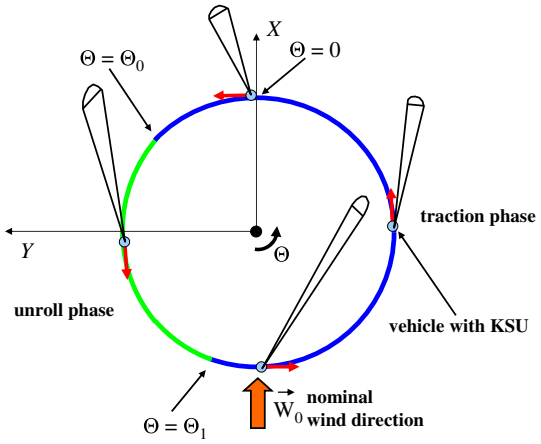

Figure 7. KE-carousel configuration phases with variable line length. KSU, Kite Steering Unit.

advantage (i.e., its angular position is greater than Θ_1 in Figure 7), the KE-carousel *traction phase* starts: the kite pulls the vehicle, and the drives linked to the wheels act as generators. Meanwhile, the kite lines are rolled back in order to always start the next unroll phase with the same line length. Thus, in the traction phase, the net generated energy is given by the difference between the energy generated by pulling the vehicle and the energy spent to recover the lines. Therefore, the controller employed in the KE-carousel with variable line length has to be designed in order to maximize such a net generated energy. The control design and simulation results of a KE-yoyo carousel with variable line length have been presented in [11], considering a fixed speed of the KSU along the carousel path. As a matter of fact, a variable vehicle speed can be exploited in the KE-carousel as an additional degree of freedom; in this paper, this possibility is investigated and compared with the KE-yoyo and KE-carousel with constant line length (Sections 3.4 and 5).

2.3. *System model*

The mathematical models of the described Kitenergy generators will now be resumed. For more details on the system model, the interested reader is referred to [11, 12, 25].

A fixed Cartesian coordinate system (X, Y, Z) is considered (Figure 8), with X axis aligned with the nominal wind speed vector direction. Wind speed vector is represented as

$$\vec{W}_l = \vec{W}_0 + \vec{W}_t, \tag{1}$$

where $\vec{W}_0$ is the nominal wind supposed to be known and expressed in (X, Y, Z) as

$$\vec{W}_0 = \begin{pmatrix} W_x(Z) \\ 0 \\ 0 \end{pmatrix}. \tag{2}$$

$W_x(Z)$ is a known function that gives the wind nominal speed at the altitude Z. The term $\vec{W}_t$ may have components in all directions and is not supposed to be known, accounting for wind unmeasured turbulence. In the performed studies, function $W_x(Z)$ corresponds to a logarithmic wind shear model (see, e.g., [2]):

$$W_x(Z) = W_{\text{ref}} \frac{\ln\left(\frac{Z}{Z_r}\right)}{\ln\left(\frac{Z_{\text{ref}}}{Z_r}\right)}, \tag{3}$$

where W_{ref}, Z_{ref}, and Z_r are the wind shear model parameters. An example of wind shear profile related to the site of Brindisi, Italy, during winter months is reported in Figure 9, where the

DOI: 10.1002/rnc

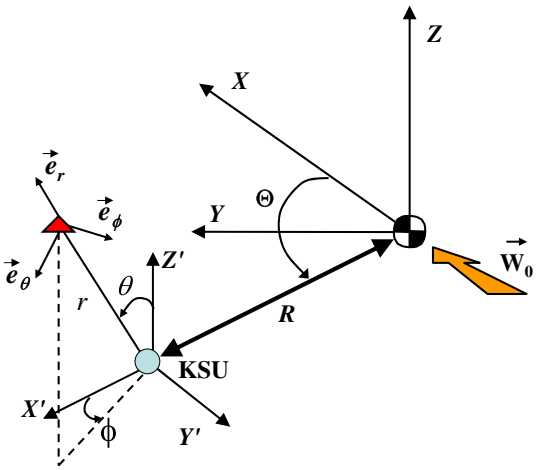

Figure 8. Model diagram of Kitenergy generators. KSU, Kite Steering Unit.

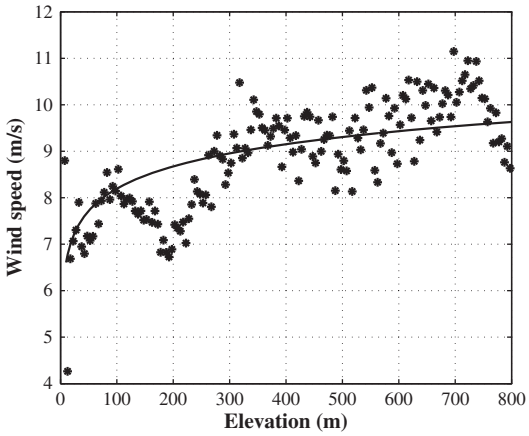

Figure 9. Wind shear model, related to the site of Brindisi (Italy) during winter months. Asterisks: experimental data; solid line: wind shear model.

parameters have been estimated as $W_{\text{ref}} = 7.4$ m/s, $Z_{\text{ref}} = 32.5$ m, and $Z_r = 6\,10^{-4}$ m using the data contained in the database RAOB (RAwinsonde OBservation, Environmental Research Services, LLC, Matamoras, PA, USA) of the National Oceanic and Atmospheric Administration [26].

A second, possibly moving, Cartesian coordinate system (X', Y', Z'), centered at the KSU location, is considered. In this system, the kite position can be expressed as a function of its distance r from the origin and of the two angles θ and ϕ, as depicted in Figure 8, which also shows the three unit vectors $\vec{e}_\theta$, $\vec{e}_\phi$, and $\vec{e}_r$ of a local coordinate system centered at the kite center of gravity. In the KE-carousel configuration, the KSU angular position Θ is defined by the direction of X and X' axes (Figure 8).

By applying Newton's laws of motion to the kite in the local coordinate system $\left(\vec{e}_\theta, \vec{e}_\phi, \vec{e}_r\right)$, the following dynamic equations are obtained:

$$\begin{aligned} \ddot{\theta} &= \frac{F_\theta}{m\,r}, \\ \ddot{\phi} &= \frac{F_\phi}{m\,r\,\sin\theta}, \\ \ddot{r} &= \frac{F_r}{m}, \end{aligned} \tag{4}$$

DOI: 10.1002/rnc

where m is the kite mass. Forces F_θ, F_ϕ, and F_r include the contributions of the gravity force acting on the kite and the lines, $\vec{F}^{\text{grav}}$, of the apparent force, $\vec{F}^{\text{app}}$, of the kite aerodynamic force, $\vec{F}^{\text{aer}}$, of the aerodynamic drag force of the lines, $\vec{F}^{\text{c,aer}}$, and of the traction force exerted by the lines on the kite, $F^{\text{c,trc}}$.

Gravity forces take into account the kite weight and the contribution given by the weight of the lines. Apparent forces include centrifugal and inertial forces because of the kite and KSU movement. The kite aerodynamic force $\vec{F}^{\text{aer}}$ can be derived via the computation of the lift and drag forces, $\vec{F}_{\text{L}}$ and $\vec{F}_{\text{D}}$, respectively:

$$\vec{F}_{\text{L}} = -\frac{1}{2} C_{\text{L}} A \rho |\vec{W}_{\text{e}}|^2 \vec{z}_{\text{w}}, \tag{5}$$

$$\vec{F}_{\text{D}} = \frac{1}{2} C_{\text{D}} A \rho |\vec{W}_{\text{e}}| \vec{W}_{\text{e}}. \tag{6}$$

In Equations (5)–(6), ρ is the air density, A is the kite area, C_{L} and C_{D} are the kite aerodynamic lift and drag coefficients, respectively, which in turn depend on the kite attack angle α, as shown in Figure 10, where the courses of $C_{\text{L}}(\alpha)$ and $C_{\text{D}}(\alpha)$ considered in this paper are depicted. It is assumed that the angle of attack of the kite can be suitably chosen during the flight, by using onboard actuators, so that the related lift and drag coefficients, resulting from the curves in Figure 10, are imposed. Finally, $\vec{W}_{\text{e}}$ is the kite effective wind speed, computed as

$$\vec{W}_{\text{e}} = \vec{W}_{\text{l}} - \vec{v}_{\text{kite}} - \vec{v}_{\text{carousel}}, \tag{7}$$

where $\vec{v}_{\text{kite}}$ and $\vec{v}_{\text{carousel}}$ are respectively the kite velocity and the carousel velocity with respect to the ground. In Equation (5), the unit vector $\vec{z}_{\text{w}}$ is perpendicular to the effective wind speed $\vec{W}_{\text{e}}$ and points down when $\vec{W}_{\text{e}}$ is parallel to the ground. According to [11], the aerodynamic drag force of the lines, $\vec{F}^{\text{c,aer}}$, can be expressed as

$$\vec{F}^{\text{c,aer}} = \frac{1}{8} C_{\text{D,l}} A_{\text{l}} \cos(\beta) \rho |\vec{W}_{\text{e}}| \vec{W}_{\text{e}}, \tag{8}$$

where $C_{\text{D,l}}$ is the cable drag coefficient, A_{l} is the cable front area, and β is the angle between the effective wind speed vector $\vec{W}_{\text{e}}$ and the plane, tangent to the sphere of radius r, which contains the kite position (i.e., the plane $(\vec{e}_\theta, \vec{e}_\phi)$, see Figure 8). By taking into account the drag forces of the kite and of the cable, the total drag force $\vec{F}_{\text{D,tot}}$ can be computed as

$$\vec{F}_{\text{D,tot}} = \vec{F}_{\text{D}} + \vec{F}^{\text{c,aer}} = \frac{1}{2} C_{\text{D}} A \rho |\vec{W}_{\text{e}}| \vec{W}_{\text{e}} + \frac{1}{8} C_{\text{D,l}} A_{\text{l}} \cos(\beta) \rho |\vec{W}_{\text{e}}| \vec{W}_{\text{e}}. \tag{9}$$

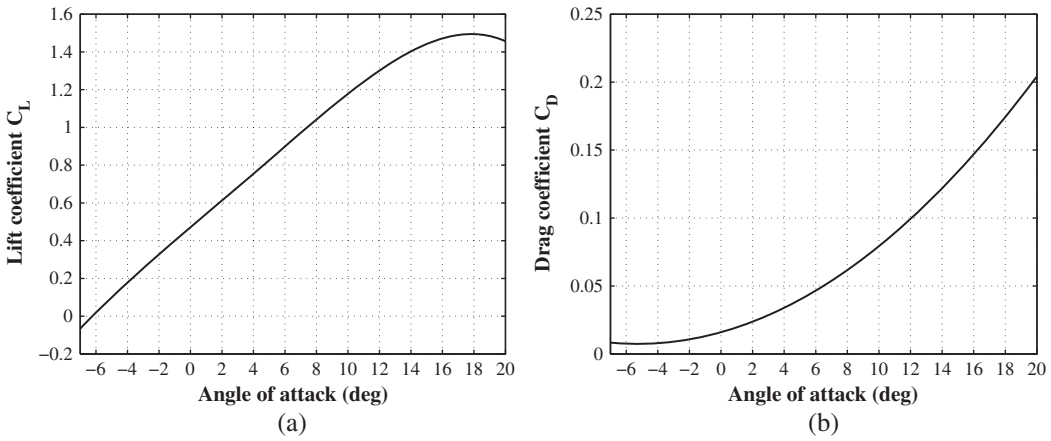

Figure 10. Aerodynamic (a) lift and (b) drag coefficients as functions of the kite angle of attack α.

DOI: 10.1002/rnc

By considering a wing with two cables of diameter d_l and length r each, that is, $A_l = 2r\,d_l$, Equation (9) becomes

$$\vec{F}_{D,tot} = \frac{1}{2}\rho A C_D \left(1 + \frac{2\,r\,d_l C_{D,l}\cos(\beta)}{4\,A\,C_D}\right)|\vec{W}_e|\,\vec{W}_e. \tag{10}$$

Let the equivalent drag coefficient $C_{D,eq}$ be defined as

$$C_{D,eq} = C_D \left(1 + \frac{2\,r\,d_l C_{D,l}\cos(\beta)}{4\,A\,C_D}\right), \tag{11}$$

then Equation (10) can be written as

$$\vec{F}_{D,tot} = \frac{1}{2}\rho A C_{D,eq}|\vec{W}_e|\,\vec{W}_e. \tag{12}$$

The control variable is the angle ψ that can influence the roll angle of the kite, thus changing the orientation of the unit vector $\vec{z}_w$ (which is always perpendicular to the effective wind speed) and, consequently, of the lift force $\vec{F}_L$. Angle ψ is defined as

$$\psi \doteq \arcsin\left(\frac{\Delta l}{d}\right), \tag{13}$$

with d being the distance between the two lines fixing points at the kite and Δl the length difference of the two lines that can be issued by a suitable control of the electric drives.

The traction force exerted by the cables on the kite, $F^{c,trc}$, is always directed along the local unit vector $\vec{e}_r$ and cannot be positive, because the lines can only pull the kite down. Moreover, $F^{c,trc}$ is measured by a force transducer on the KSU and, with the use of a local controller of the electric drives, it is regulated in such a way that $\dot{r}(t) = \dot{r}_{ref}(t)$, where $\dot{r}_{ref}(t)$ is the reference line speed.

In the case of KE-carousel configuration, the motion law of the KSU along the circular path of radius R has to be included too, with the following equation:

$$M\ddot{\Theta}R = F^{c,trc}\sin\theta\sin\phi - F^{gen}, \tag{14}$$

where M is the total mass of the vehicle and F^{gen} is the force exerted by the electric drives linked to the wheels. It is supposed that suitable kinematic constraints (e.g., rails) oppose to the centrifugal inertial force acting on the vehicle and to all of the components of the line force, except for the one acting along the tangent to the vehicle path (i.e., $F^{c,trc}\sin\theta\sin\phi$). Note that any viscous term is neglected in Equation (14), because the vehicle speed $\dot{\Theta}R$ will be kept very low. The force F^{gen} is positive when the kite is pulling the vehicle towards increasing Θ values, thus generating energy, and it is negative when the electric drives are acting as motors to drag the vehicle against the wind when the kite is not able to generate a suitable pulling force.

By considering that the kite altitude Z depends on r and θ, that is,

$$Z = r\cos(\theta), \tag{15}$$

the model equations (1)–(15) give the system dynamics in the form

$$\dot{x}(t) = f\left(x(t), u(t), \dot{r}_{ref}(t), \dot{\Theta}_{ref}(t), \alpha, \vec{W}_t(t)\right), \tag{16}$$

where $x(t) = \left[\theta(t)\;\phi(t)\;r(t)\;\Theta(t)\;\dot{\theta}(t)\;\dot{\phi}(t)\;\dot{r}(t)\;\dot{\Theta}(t)\right]^T$ are the model states and $u(t) = \psi(t)$ is the control input. Clearly, in the case of KE-yoyo configuration, $\Theta = \dot{\Theta} = \dot{\Theta}_{ref} = 0$. The net mechanical power P generated (or spent) is the algebraic sum of the power generated (or spent) by unrolling/recovering the lines and by the vehicle movement:

$$P(t) = \dot{r}(t)F^{c,trc}(t) + \dot{\Theta}(t)\,R\,F^{gen}(t). \tag{17}$$

Indeed, for the KE-yoyo configuration the term $\dot{\Theta}\,R\,F^{gen} = 0$ and the generated mechanical power is only due to line unrolling, whereas for the KE-carousel with fixed cable length, the term $\dot{r}(t) = 0$ and the generated power is related to the KSU movement only.

DOI: 10.1002/rnc

2.4. Control requirements and controller design

Advanced control techniques are fundamental to operate airborne power generators. In fact, the kite flight has to be stabilized and suitably controlled to continuously perform the different operational phases of the KE-yoyo or KE-carousel configurations. In each of the working phases, the objective to be achieved can be formulated as an optimization problem with its own cost function and with state and input constraints in order to prevent the kite from getting too close to the ground and to avoid line wrapping and interference among more kites flying close in the same area. Then, a suitable control strategy, able to achieve the required objective while avoiding constraint violation, has to be employed. To this end, nonlinear model predictive control (NMPC; see, e.g., [27]) techniques are employed because they are able to take into account state and input constraints.

Control design and simulation results are described in [11, 12], where it is shown that the NMPC control laws are very effective, giving a generated power of up to 10 MW with a single KSU unit equipped with a 500-m^2-size kite with an aerodynamic efficiency of 8–10 and wind speed of 15 m/s. These studies allow one to estimate that wind farms based on Kitenergy technology can have energy generation costs significantly lower than fossil sources, as shown in Table I (reported from [12]), where a comparison is made with the costs of other energy generation technologies as evaluated in [28]. Moreover, the first experimental results (see movies [29, 30]) obtained with a small-scale prototype show a good matching with the employed model, thus increasing the confidence in the previously reported cost estimates [11, 12].

2.5. Problem description

In this paper, we investigate some further questions arising in the control design of Kitenergy technology.

- In each working phase, the NMPC approach requires the solution of an optimization problem that, being the model nonlinear, may be not convex, and the numerical optimization algorithm may be trapped in local minima. Moreover, in order to limit the computational complexity, the prediction horizon considered in the NMPC design is much shorter than the duration of the phase. Thus, it is important to evaluate how far the obtained performance is from the optimality of the whole generation cycle.
- The overall control strategy requires the designing of not only the control law $u(t_k)$ but also several 'operational' parameters (e.g., $\dot{r}_{\text{ref}}$ and $\dot{\Theta}_{\text{ref}}$) that have to be set up according to the wind speed, wing and cable features, and so on in order to maximize the generated energy over the whole generation cycle. It would be useful to have a systematic and a simple way to optimally compute such operational parameters.
- In the KE-yoyo and in the KE-carousel with fixed cable length, the energy generation is not constant because of the periodic cycling between traction and passive phases. It is of interest to evaluate if it is possible to realize a Kitenergy generator that does not require passive phases, so that the net energy production is constant and possibly maximal.

Table I. Projected cost in 2030 (levelized in 2003) of energy from different sources compared with the estimated energy cost of KiteEnergy.

Source	Minimal estimated ($/MWh)	Maximal estimated ($/MWh)	Average estimated ($/MWh)
Coal	25	50	34
Gas	37	60	47
Nuclear	21	31	29
Wind	35	95	57
Solar	180	500	325
Kitenergy	10	48	20

DOI: 10.1002/rnc

The key idea for answering these questions is to employ simplified equations that give the generated power as a function of all of the main involved operational parameters and variables, together with optimization techniques, to derive the operating conditions that achieve the maximal generated power. However, such equations are based on simplified hypotheses (for example, inertial forces are neglected) that, in general, lead to higher power values than the ones derived by the much more detailed dynamical model described in Section 2.3. Indeed, as shown in the following, such overbounding is quite moderate. As an original contribution of this paper, such a procedure is applied to evaluate whether the NMPC strategy is able to achieve optimal energy generation performance and is able to optimally design the operational cycles of a KE-yoyo and of a KE-carousel with either fixed or variable line length. Such optimization procedures will be carried out either numerically or analytically. Then, numerical simulations with the use of the optimized parameters will be carried out in Section 4 in order to assess the matching between the results obtained by the simplified equations with those given by the dynamical model (16).

3. OPTIMIZATION OF AIRBORNE WIND ENERGY GENERATORS

In this section, simplified equations of kite power are presented and employed to optimize the operational cycles of Kitenergy generators.

3.1. Simplified equations of kite power

Consider a wing linked to a point at ground level (i.e., the KSU). Indicate with r the cable length and with $\vec{e}_r$ a unit vector parallel to the cable and pointing towards increasing r values (Figure 11). Moreover, indicate with $\vec{W}_{\mathrm{e,p}}$ the projection of $\vec{W}_{\mathrm{e}}$ on the plane $(\vec{e}_\theta, \vec{e}_\phi)$, which is perpendicular to vector $\vec{e}_r$. From Equations (5) and (12), the magnitudes of the wing lift and drag forces, $|\vec{F}_{\mathrm{L}}|$ and $|\vec{F}_{\mathrm{D,tot}}|$, respectively, are

$$\begin{aligned} |\vec{F}_{\mathrm{L}}| &= \frac{1}{2}\rho A C_{\mathrm{L}} |\vec{W}_{\mathrm{e}}|^2, \\ |\vec{F}_{\mathrm{D,tot}}| &= \frac{1}{2}\rho A C_{\mathrm{D,eq}} |\vec{W}_{\mathrm{e}}|^2. \end{aligned} \tag{18}$$

Then, an equivalent kite aerodynamic efficiency can be defined as

$$E_{\mathrm{eq}} \doteq \frac{|\vec{F}_{\mathrm{L}}|}{|\vec{F}_{\mathrm{D,tot}}|} = \frac{C_{\mathrm{L}}}{C_{\mathrm{D,eq}}}. \tag{19}$$

Remark 1

It is worth noting that the equivalent kite aerodynamic efficiency E_{eq} defined in Equation (19) depends on the cable length r and on the angle β, because the equivalent drag coefficient $C_{\mathrm{D,eq}}$ in Equation (11) depends on both these variables.

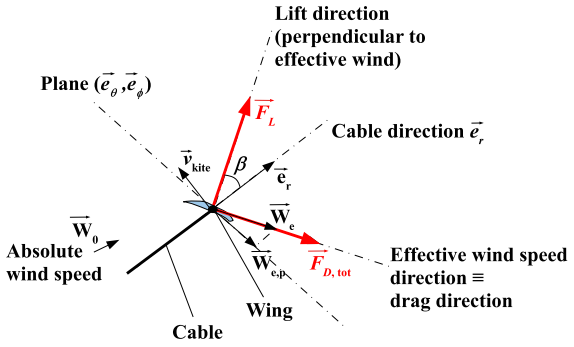

Figure 11. Sketch of a wing flying in crosswind conditions.

DOI: 10.1002/rnc

In order to derive simplified kite power equations that will be exploited to analyze the performance of the KE-systems, the following assumptions are considered.

Assumption 1
The kite flies in crosswind conditions, as considered in [8].

Assumption 2
The inertial and apparent forces are negligible with respect to the aerodynamic forces.

Assumption 3
The kite speed relative to the ground is constant.

Assumption 4
The kite speed relative to the ground is much higher than the speed of the KSU relative to the ground.

Assumption 5
The kite aerodynamic lift force $\vec{F}_{\mathrm{L}}$ approximately lies on the plane defined by vectors $\vec{W}_{\mathrm{e,p}}$ and $\vec{e}_r$.

Assumption 6
The component of the lift force vector $\vec{F}_{\mathrm{L}}$ along the direction of $\vec{e}_r$ is positive, that is, the angle β assumes values in the interval $[0, \pi/2)$.

Basically, Assumptions 1–6 imply that the wing is flying at a high speed in crosswind conditions and that its lift force is being exploited to pull the cables.

Proposition 1
If Assumptions 1–5 hold, then the following equation involving the angle β holds:

$$\frac{\sin(\beta)}{\cos(\beta)} = \frac{1}{E_{\mathrm{eq}}(\beta)}. \tag{20}$$

Proof
See Appendix □

Corollary 1
Furthermore, if Assumption 6 also holds, then there is only one value of $\beta \in [0, (\pi/2) - \varepsilon]$ satisfying Equation (20).

Proof
See Appendix □

Note that, in view of Corollary 1, the value of β satisfying Equation (20) can be easily computed by means of numerical methods, (e.g., bisection or Newton–Raphson method).

Proposition 2
If Assumptions 1–6 hold, then the total traction force $F^{\mathrm{c,trc}}$ acting on the cables can be computed as

$$F^{\mathrm{c,trc}} = \frac{1}{2}\rho A C_{\mathrm{L}} E_{\mathrm{eq}}^2 \left(1 + \frac{1}{E_{\mathrm{eq}}^2}\right)^{\frac{3}{2}} |\vec{W}_{\mathrm{e},r}|^2 = C\,|\vec{W}_{\mathrm{e},r}|^2, \tag{21}$$

where

$$C = \frac{1}{2}\rho A C_{\mathrm{L}} E_{\mathrm{eq}}^2 \left(1 + \frac{1}{E_{\mathrm{eq}}^2}\right)^{\frac{3}{2}}, \tag{22}$$

DOI: 10.1002/rnc

and $|\vec{W}_{e,r}|$ is the magnitude of the projection of the effective wind speed on the cable direction, computable as

$$\vec{W}_{e,r} = |\vec{W}_0(r,\theta)| \sin(\theta) \cos(\phi + \Theta) - \dot{r} - R\dot{\Theta} \sin(\phi). \tag{23}$$

Proof
See Appendix □

Equation (21) gives the traction force on the cable as a function of the effective wind speed projected on the cable itself. Note that Equation (21) gives an upper bound of the traction force that can be generated by the kite. Thus, Equation (21) can be employed to study the optimal operating conditions of the system in order to compute an upper bound of the maximal generated power.

Remark 2
The equation of traction force $F^{c,trc}$ (Equation (21)) is more general with respect to other expressions previously computed in literature (see, e.g., [8, 12, 31]), because in Equation (21), both the drag effect of the cables and the mutual dependance between the drag force and the angle β are considered. By neglecting the cable drag, the result of [8] is obtained.

3.2. Optimization of a KE-yoyo generator

As described in Section 2.2, the operation of a KE-yoyo is divided into two phases, the traction and the passive ones. The operational parameters are the values θ_{trac}, ϕ_{trac} and θ_{pass}, ϕ_{pass} of angles θ, ϕ during the traction and passive phases, the minimal cable length $\underline{r}$ during the cycle, and the cable speed during the traction and the passive phase, $\dot{r}_{trac}$ and $\dot{r}_{pass}$, respectively. In the traction phase, a suitable angle of attack α_{trac} is issued by the onboard actuators, in order to have high wing efficiency and lift coefficient. Then, during the passive phase, the angle of attack is changed to a value α_{pass} giving low lift and efficiency, so that the lines can be rolled back under low traction forces.

By indicating with $P_{trac}(t)$ and $P_{pass}(t)$ the power generated (or spent) in the traction and passive phases, respectively, the average power $\overline{P}$ obtained in a cycle can be computed as:

$$\overline{P} = \frac{\int_{t_0}^{t_{trac,end}} P_{trac}(\tau)\,d\tau + \int_{t_{trac,end}}^{t_{pass,end}} P_{pass}(\tau)\,d\tau}{t_{pass,end} - t_0}, \tag{24}$$

where t_0 and $t_{trac,end}$ are the starting and ending instants of the traction phase, whereas $t_{pass,end}$ is the ending instant of the passive phase (in this analysis, it is assumed that the starting instant of the passive phase coincides with the ending instant of the traction one). The following assumptions are considered.

Assumption 7
Approximately constant angles θ_{trac} and θ_{pass} , as well as constant angles ϕ_{trac} and ϕ_{pass}, during the traction and passive phases are kept.

Assumption 8
Constant cable unrolling speed $\dot{r}_{trac} > 0$ and winding back speed $\dot{r}_{pass} < 0$ are employed during the traction and passive phases, respectively.

Assumption 9
The amplitude Δr of the variation of the cable length r during each cycle, which occurs at the beginning of each traction phase, is imposed, and it is relatively small (e.g., 50 m) with respect to the minimal cable length $\underline{r}$ (e.g., 800–1000 m).

DOI: 10.1002/rnc

Proposition 3
If Assumptions 1–9 hold, then the average power $\overline{P}$ in Equation (24) can be computed as

$$\overline{P} = \left(F_{\text{trac}}^{\text{c,trc}} - F_{\text{pass}}^{\text{c,trc}}\right) \frac{\dot{r}_{\text{trac}}\, \dot{r}_{\text{pass}}}{\dot{r}_{\text{pass}} - \dot{r}_{\text{trac}}}. \tag{25}$$

Proof
See Appendix □

Equation (25) can be used to optimally design the KE-yoyo operating parameters. Indeed, the values of the forces $F_{\text{trac}}^{\text{c,trc}}$ and $F_{\text{pass}}^{\text{c,trc}}$ depend on the parameters to be optimized θ_{trac}, ϕ_{trac}, θ_{pass}, ϕ_{pass}, $\underline{r}$, $\dot{r}_{\text{trac}}$, $\dot{r}_{\text{pass}}$, according to Equations (21)–(23). In fact, the traction force can be expressed as

$$F^{\text{c,trc}}(\theta, \phi, \dot{r}, r) = C(r)\left(|\vec{W}_0(r, \theta_{\text{trac}})| \sin(\theta)\cos(\phi) - \dot{r}\right)^2.$$

It can be noted that the value of ϕ that gives the maximal traction force is $\phi^* = 0$, as it can be derived also by intuition, because $\phi = 0$ means that the wing is flying perfectly downwind. Thus, the value $\phi_{\text{trac}} = 0$ is chosen in order to maximize the cable force during the traction phase of the KE-yoyo. During the passive phase, in principle, it would be useful to use a high absolute value of angle ϕ (i.e., to move the kite in a lateral position with respect to the wind direction) to reduce the cable forces. However, such a solution would require spending more time, between the traction and passive phases, to drive the kite in the chosen position, thus decreasing the average energy generated during the cycle. Moreover, the angle of attack α_{pass} issued during the passive phase is such that the resulting traction forces are very low, and the effects of large ϕ angles are negligible. Therefore, the value $\phi_{\text{pass}} = 0$ is chosen for the passive phase. With the chosen values of ϕ, the cable forces during the traction and passive phases can be computed as

$$\begin{aligned} F_{\text{trac}}^{\text{c,trc}}(\theta_{\text{trac}}, \dot{r}_{\text{trac}}, \underline{r}) &= C_{\text{trac}}(\underline{r})\left(|\vec{W}_0(r, \theta_{\text{trac}})| \sin(\theta_{\text{trac}}) - \dot{r}_{\text{trac}}\right)^2, \\ F_{\text{pass}}^{\text{c,trc}}(\theta_{\text{pass}}, \dot{r}_{\text{pass}}, \underline{r}) &= C_{\text{pass}}(\underline{r})\left(|\vec{W}_0(r, \theta_{\text{pass}})| \sin(\theta_{\text{pass}}) - \dot{r}_{\text{pass}}\right)^2, \end{aligned} \tag{26}$$

where the values of C_{trac} and C_{pass} are computed by using Equation (22), by considering the aerodynamic coefficients corresponding to the values of angle of attack α_{trac} and α_{pass} respectively, (see Section 2.3 and Figure 10).

Therefore, the following optimization problem can be considered to design the operational parameters of the KE-yoyo:

$$\left(\theta_{\text{trac}}^*, \dot{r}_{\text{trac}}^*, \underline{r}^*, \theta_{\text{pass}}^*, \dot{r}_{\text{pass}}^*\right) = \arg\max \overline{P}\left(\theta_{\text{trac}}, \dot{r}_{\text{trac}}, \underline{r}, \theta_{\text{pass}}, \dot{r}_{\text{pass}}\right).$$

Furthermore, operational constraints have to be taken into account in the optimization in order to find out feasible operating conditions. In particular, the involved constraints regard the maximal and minimal cable unrolling/rewinding speed, the minimal elevation of the wing from the ground (considering also its maneuvering radius), the minimal angle θ during the cycle, and the cable breaking force. The constraints on the line speed are

$$\dot{r}_{\min} \leqslant \dot{r} \leqslant \min\left(|\vec{W}_0(r, \theta_{\text{trac}})| \sin(\theta), \dot{r}_{\max}\right),$$

where $\dot{r}_{\min}$ and $\dot{r}_{\max}$ are imposed by the limitations of the electric drives employed on the KSU and by the need to prevent excessive cable wear because of the high unrolling/rewinding speed, whereas the constraint $\dot{r} \leqslant |\vec{W}_0(r, \theta_{\text{trac}})| \sin(\theta)$ has been included in order to ensure that the kite exerts a positive traction force on the cables. Besides, in order to impose a minimal elevation $\underline{Z}$ of the kite, the minimum value of the maneuvering radius R_{F} during the kite flight ought to be taken into account. In particular, because R_{F} depends on the wingspan w_s of the kite, according to the approximate relationship $R_{\text{F}} \simeq 2.5 w_s$, the minimal elevation $\underline{Z}$ can be imposed by requiring that (Figure 12)

DOI: 10.1002/rnc

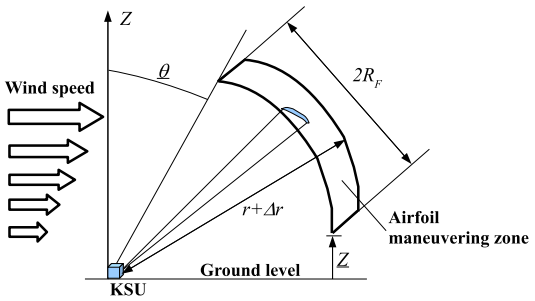

Figure 12. KE-yoyo operation: constraints on minimal elevation Z and on minimal angle θ. KSU, Kite Steering Unit.

$$\underline{r}\cos\left(\theta+\frac{R_{\mathrm{F}}}{\underline{r}+\Delta r}\right)\geqslant\underline{Z}. \tag{27}$$

A constraint on the minimal value of θ is also introduced in order to keep the wing trajectory contained in a relatively small area and to obtain short idle time intervals between the traction and recovery phases:

$$\theta\geqslant\underline{\theta},$$

with $0\leqslant\underline{\theta}\leqslant\pi/2$. Finally, the constraint related to the cable breaking load can be expressed, for two cables with a given cable diameter d_{l}, as

$$F_{\mathrm{trac}}^{\mathrm{c,trc}}\leqslant 2\frac{\overline{F}(d_{\mathrm{l}})}{c_{\mathrm{s}}},$$
$$F_{\mathrm{pass}}^{\mathrm{c,trc}}\leqslant 2\frac{\overline{F}(d_{\mathrm{l}})}{c_{\mathrm{s}}},$$

where $\overline{F}(\cdot)$ is the minimum breaking force of a single cable (which depends on the cable material and diameter; see, e.g., [12] for details) and c_{s} is a safety coefficient.

By considering all of the described constraints, the optimization problem to be solved is given by

$$\begin{gathered}\left(\theta_{\mathrm{trac}}^{*},\dot{r}_{\mathrm{trac}}^{*},\underline{r}^{*},\theta_{\mathrm{pass}}^{*},\dot{r}_{\mathrm{pass}}^{*}\right)=\arg\max\overline{P}\left(\theta_{\mathrm{trac}},\dot{r}_{\mathrm{trac}},\underline{r},\theta_{\mathrm{pass}},\dot{r}_{\mathrm{pass}}\right),\\ \text{s. t.}\\ \dot{r}_{\min}\leqslant\dot{r}\leqslant\min\left(|\vec{W}_0(r,\theta)|\sin(\theta),\dot{r}_{\max}\right),\\ \underline{r}\cos\left(\theta+\tfrac{R_{\mathrm{F}}}{\underline{r}}\right)\geqslant\underline{Z},\\ \theta\geqslant\underline{\theta},\\ F_{\mathrm{trac}}^{\mathrm{c,trc}}\leqslant 2\tfrac{\overline{F}(d_{\mathrm{l}})}{c_{\mathrm{s}}},\\ F_{\mathrm{pass}}^{\mathrm{c,trc}}\leqslant 2\tfrac{\overline{F}(d_{\mathrm{l}})}{c_{\mathrm{s}}}.\end{gathered} \tag{28}$$

With the system data given in Table II and considering the aerodynamic characteristics of Figure 10 and the wind shear profile reported in Figure 9, the solution of the optimization problem (Equation (28)) is the following:

$$\begin{pmatrix}\theta_{\mathrm{trac}}^{*}\\ \dot{r}_{\mathrm{trac}}^{*}\\ \underline{r}^{*}\\ \theta_{\mathrm{pass}}^{*}\\ \dot{r}_{\mathrm{pass}}^{*}\end{pmatrix}=\begin{pmatrix}69.1^{\circ}\\ 2.14\,\mathrm{m/s}\\ 631\,\mathrm{m}\\ 50^{\circ}\\ -6.0\,\mathrm{m/s}\end{pmatrix}. \tag{29}$$

DOI: 10.1002/rnc

Table II. Optimization of a KE-yoyo operational cycle with low-lift maneuver: system parameters.

A	500 m^2	Characteristic area
d_l	0.04 m	Diameter of a single line
$\overline{F}(d_\mathrm{l})$	1.50 10^6 N	Minimum breaking load of a single line
α_trac	12°	Angle of attack during the traction phase ($C_\mathrm{L} = 1.3$, $C_\mathrm{D} = 0.1$)
α_pass	−6°	Angle of attack during the passive phase ($C_\mathrm{L} = 0.02$, $C_\mathrm{D} = 0.08$)
ρ	1.2 kg/m^3	Air density
Δr	50 m	Maximum line variation during a cycle
$\dot{r}_\mathrm{min}$	−6 m/s	Minimal line speed
$\dot{r}_\mathrm{max}$	6 m/s	Maximal line speed
$\underline{Z}$	30 m	Minimal elevation from the ground
$\underline{\theta}$	50°	Minimal angle θ
c_s	2	Safety coefficient
w_s	80 m	Kite wingspan

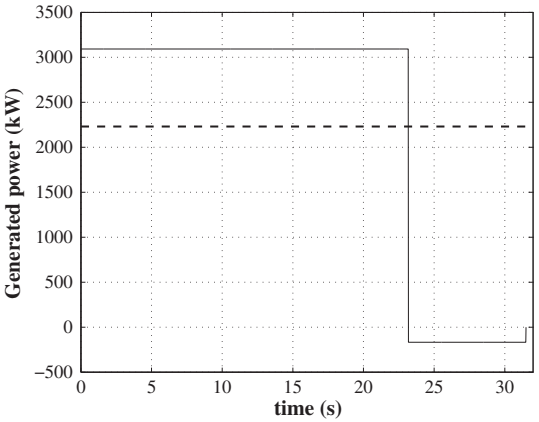

Figure 13. Optimized operation of a KE-yoyo with low-lift maneuver in one complete cycle, computed using the simplified power equations. Mean (dashed) and actual (solid) generated power.

The related course of the generated power is shown in Figure 13. The corresponding optimal average power value is equal to 2.2 MW.

3.3. Optimization of a KE-carousel generator with constant cable length and vehicle speed

In the KE-carousel with constant cable length, power is generated by the vehicle movement. The line rolling speed $\dot{r}$ is equal to zero, whereas the tangential speed $R\dot{\Theta}$ is kept constant. Thus, the angular acceleration $\ddot{\Theta}$ is zero and, from Equation (14), the force F^gen is

$$F^\mathrm{gen} = F^\mathrm{c,trc} \sin(\theta) \sin(\phi).$$

Moreover, from Equation (17) and because $\dot{r} = 0$, the generated power $P^\mathrm{const}_\mathrm{KE\text{-}carousel}$ is

$$P^\mathrm{const}_\mathrm{KE\text{-}carousel} = F^\mathrm{gen} R\dot{\Theta} = F^\mathrm{c,trc} \sin(\theta) \sin(\phi) R\dot{\Theta}. \tag{30}$$

By combining Equations (21), (23), and (30), the following expression of $P^\mathrm{const}_\mathrm{KE\text{-}carousel}$ is obtained:

$$P^\mathrm{const}_\mathrm{KE\text{-}carousel} = C(r) \left| \vec{W}_{\mathrm{e},r} \right|^2 \sin(\theta) \sin(\phi) R\dot{\Theta}.$$

DOI: 10.1002/rnc

The instantaneous generated power $P^{\text{const}}_{\text{KE-carousel}}$ depends on the KE-carousel angular position Θ, and the mean power $\bar{P}^{\text{const}}_{\text{KE-carousel}}$ generated during the whole cycle can be computed as

$$\bar{P}^{\text{const}}_{\text{KE-carousel}} = \frac{1}{t_{\text{end,cr}}} \int_0^{t_{\text{end,cr}}} P^{\text{const}}_{\text{KE-carousel}}\left(\Theta(t)\right) \mathrm{d}t, \tag{31}$$

where $\Theta(0) = 0$ and $t_{\text{end,cr}}$ is the final time of the carousel cycle, that is, $\Theta(t_{\text{end,cr}}) = 2\pi$.

Because the carousel moves at constant speed, by discretizing the carousel path with the use of N points, Equation (31) can be approximated as

$$\bar{P}^{\text{const}}_{\text{KE-carousel}} \simeq \frac{1}{N} \sum_{i=1}^{N} P^{\text{const}}_{\text{KE-carousel}}\left(\Theta_i\right). \tag{32}$$

Equation (32) allows one to convert the infinite dimensional objective function (Equation (31)) into a finite dimensional one. Like the case of the KE-yoyo analysis (Equation (27)), a minimum elevation $\underline{Z}$ of the kite during its flight has to be imposed by requiring that

$$r \cos\left(\theta + \frac{R_{\text{F}}}{r}\right) \geqslant \underline{Z}. \tag{33}$$

Moreover, similarly to the case of a KE-yoyo, the constraint related to the cable breaking load is expressed, for two cables with a given diameter d_{l}, as

$$F^{\text{c,trc}} \leqslant 2\frac{\bar{F}(d_{\text{l}})}{c_{\text{s}}}. \tag{34}$$

On the basis of Equation (32) and of the described constraints, an approximation of the maximum mean generated power is computed by solving the constrained optimization problem:

$$\bar{P}^{\text{const}*}_{\text{KE-carousel}} = \max_{\substack{r,\dot{\Theta},\theta_i,\phi_i \\ i=1,\ldots,N}} \frac{1}{N} \sum_{i=1}^{N} P^{\text{const}}_{\text{KE-carousel}}\left(r,\dot{\Theta},\theta_i,\phi_i,\Theta_i\right), \tag{35a}$$

$$\text{s. t.} \tag{35b}$$

$$\theta_i \geqslant 0 \quad i = 1,\ldots,N, \tag{35c}$$

$$F_i^{\text{c,trc}} \leqslant 2\frac{\bar{F}(d_{\text{l}})}{c_{\text{s}}} \quad i = 1,\ldots,N, \tag{35d}$$

$$r \cos\left(\theta_i + \frac{R_{\text{F}}}{r}\right) \geqslant \underline{Z} \quad i = 1,\ldots,N, \tag{35e}$$

$$\sin(\theta)\left(W_x \cos(\Theta_i + \phi_i) - R\dot{\Theta}\sin(\phi_i)\right) \geqslant 0 \quad i = 1,\ldots,N, \tag{35f}$$

where θ_i and ϕ_i are the values of the angles θ and ϕ at the carousel angular position Θ_i and $F_i^{\text{c,trc}}$ is the related traction force acting on the cables. Constraint (35f) has been included in order to ensure that the kite exerts a positive traction force on the cables.

With the use of the system data reported in Table III and the wind shear profile reported in Figure 9, with $N = 50$, the optimal vehicle tangential velocity $R\dot{\Theta}^*$ and optimal cable length r^* are

$$\begin{pmatrix} R\dot{\Theta}^* \\ r^* \end{pmatrix} = \begin{pmatrix} 3.98\ \text{m/s} \\ 375\ \text{m} \end{pmatrix}, \tag{36}$$

while the optimal trajectories of the angles θ and ϕ (as function of the KE-carousel angular position Θ) are reported in Figure 14(a) and 14(b), respectively. The optimal mean generated power $\bar{P}^{\text{const}*}_{\text{KE-carousel}}$ is equal to 1.89 MW. The values of the corresponding instantaneous generated power

DOI: 10.1002/rnc

Table III. Model parameters employed to compute an optimal KE-carousel cycle with constant cable length.

A	500 m^2	Characteristic area
R	300 m	KE-carousel radius
α	12°	Angle of attack ($C_L = 1.3$, $C_D = 0.1$)
d_l	0.04 m	Diameter of a single line
$C_{D,l}$	1	Line drag coefficient
ρ	1.2 kg/m^3	Air density
$\underline{Z}$	30 m	Minimal elevation from the ground
c_s	2	Safety coefficient
w_s	80 m	kite wingspan

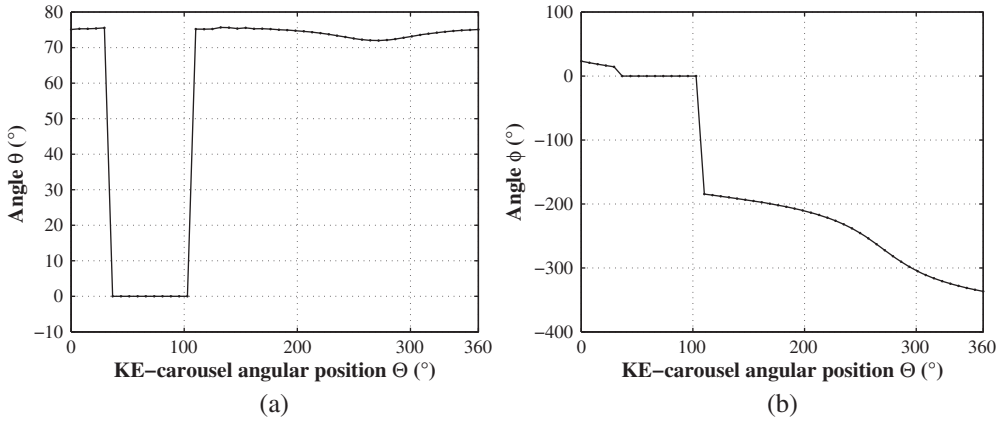

Figure 14. Optimized operation conditions of a KE-carousel with constant cable length, computed using the simplified power equations: (a) angle θ and (b) angle ϕ during the whole KE-carousel cycle.

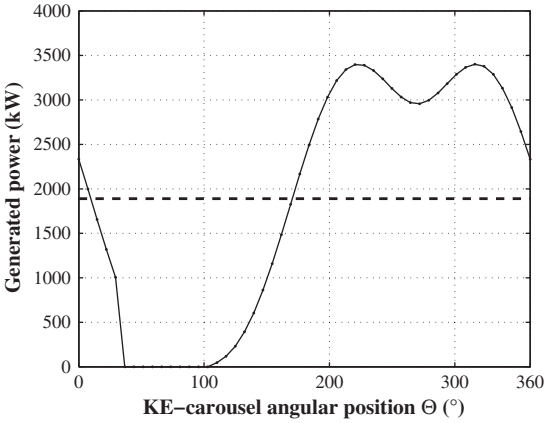

Figure 15. Optimized operation conditions of a KE-carousel with constant cable length, computed using the simplified power equations. Mean (dashed) and actual (solid) generated power.

$P^{\text{const}}_{\text{KE-carousel}}$ as function of the angle Θ is reported in Figure 15. As can be seen in Figure 14(a), for values of the angular position Θ between 35° and 110° (corresponding to the passive phase), the generated power is zero, because the angle θ is equal to zero, leading to a traction force on the cables $F^{\text{c,trc}}$ equal to zero. This means that, in this phase, the kite is not exerting any force in the direction of the vehicle longitudinal velocity, so that, ideally, no power is generated or dissipated.

DOI: 10.1002/rnc

On the other hand, in the traction phase, the angle θ is about 75°, and the angle ϕ is such that the kite pulls the vehicle, thus generating energy.

3.4. Optimization of a KE-carousel generator with variable cable length and vehicle speed

In this section, the third of the questions posed earlier, that is, if it is possible to design a KE-carousel configuration that does not require passive phases so that the net energy production is constant and at its possible maximum, is investigated. In order to simplify the analysis, the following assumptions are considered.

Assumption 10
The absolute wind speed $\vec{W}_0$ (introduced in Section 2.3) is independent on elevation and is parallel with respect to the ground.

Assumption 11
The inertial force due to the angular acceleration $\ddot{\Theta}$ is supposed to be negligible (i.e., $\ddot{\Theta} = 0$) with respect to the traction force $F^{\mathrm{c,trc}}$ acting on the cables and to the force F^{gen} exerted by the electric drives linked to the wheels.

Under Assumption 10, it can be shown that, in the two previous Kitenergy configurations, the maximal power that can be obtained using the simplified equations is

$$\max_t P(t) = C\,\frac{4}{27}|\vec{W}_0|^3. \tag{37}$$

However, the average power is lower, because in the course of time, lower values are obtained in the passive phases. Here, the operation of the KE-carousel with variable line length will be analytically optimized, and it will be shown that, by imposing suitable periodic courses of the carousel velocity and line unrolling speed, it is possible to achieve a constant net generated power equal to the theoretical upper bound (Equation (37)). On the basis of Assumptions 10–11, through straightforward manipulations of Equations (14), (17), (21), and (23), the overall power generated by a KE-carousel in a given angular position can be computed as

$$P^{\mathrm{var}}_{\text{KE-carousel}} = C\left(\sin(\theta)\left(|\vec{W}_0|\cos(\Theta+\phi) - R\,\dot{\Theta}\sin(\phi)\right) - \dot{r}\right)^2\left(\dot{r} + R\,\dot{\Theta}\sin\theta\sin\phi\right). \tag{38}$$

Then, for given values of angular position Θ and tangential speed $R\,\dot{\Theta}$, it is possible to compute the maximal overall power by solving the optimization problem

$$\begin{gathered} P^{*\mathrm{var}}_{\text{KE-carousel}}\left(\Theta,\dot{\Theta}\right) = \max_{\theta,\phi,\dot{r}} P^{\mathrm{var}}_{\text{KE-carousel}} \\ \text{s. t.} \\ \dot{r} \leqslant \sin(\theta)\left(|\vec{W}_0|\cos(\Theta+\phi) - R\,\dot{\Theta}\sin(\phi)\right), \end{gathered} \tag{39}$$

where the constraint on $\dot{r}$ has been included in order to ensure that the kite exerts a positive traction force on the cables.

Proposition 4
The global optimal solution $P^{*\mathrm{var}}_{\text{KE-carousel}}$ to optimization problem (39) is independent on the angular position Θ and tangential speed $R\,\dot{\Theta}$, and it is equal to

$$P^{*\mathrm{var}}_{\text{KE-carousel}} = \frac{4}{27}C\,|\vec{W}_0|^3. \tag{40}$$

Moreover, the optimizer $(\theta^*, \phi^*, \dot{r}^*)^T$ for Equation (39) is

$$\begin{pmatrix} \theta^* \\ \phi^* \\ \dot{r}^* \end{pmatrix} = \begin{pmatrix} \frac{\pi}{2} \\ -\Theta \\ \frac{|\vec{W}_0|}{3} + R\,\dot{\Theta}\sin(\Theta) \end{pmatrix}. \tag{41}$$

DOI: 10.1002/rnc

Proof
See Appendix □

Thus, according to Proposition 4, in any KE-carousel operating condition (in terms of Θ and $\dot{\Theta}$) a constant value of the generated power in Equation (38) can be achieved by choosing θ, ϕ, and $\dot{r}$ given by Equation (41). Now, an optimal KE-carousel operating cycle can be designed by choosing a suitable course of the vehicle angular speed $\dot{\Theta}$, such that a periodic course of all the involved variables is achieved. In particular, it is needed that the average value of $\dot{r}$ over a complete cycle equals zero.

Proposition 5
If the carousel angular speed $\dot{\Theta}$ is such that

$$\dot{\Theta} = \frac{2}{3R}|\vec{W}_0|(1 - \sin(\Theta)) \tag{42}$$

and $\dot{r}$ is equal to the optimal value $\dot{r}^*$ in Equation (41), then the average value of $\dot{r}$ over a complete cycle equals zero, that is,

$$\frac{1}{2\pi}\int_0^{2\pi} (\dot{r}(\Theta))\, \mathrm{d}\Theta = 0. \tag{43}$$

Proof
See Appendix □

The optimal courses of $\dot{\Theta}$ and $\dot{r}$ and of the power P_{vehicle} and P_{line} generated by the vehicle motion and by the line unrolling, respectively, as well as the overall optimal power $P^*_{\text{KE-carousel}}$, are reported in Figure 16(a,b) as functions of the vehicle angular position Θ. The considered KE-carousel characteristics are reported in Table IV. The overall power is constant and equal to $(4/27)C|\vec{W}_0|^3 = 3.4$ MW, that is, the maximal power is continuously obtained. Note that the wind conditions in Table IV approximately correspond to the average wind at the kite altitude in the optimized KE-yoyo and constant-cable KE-carousel presented in Sections 3.2 and 3.3, whose average power values were 2.2 and 1.89 MW, respectively. As it can be noted in Figure 16(a), the optimal cycle is such that $\dot{\Theta} = 0$ when $\Theta = \pi/2$, meaning that the vehicle should stop at such an angular

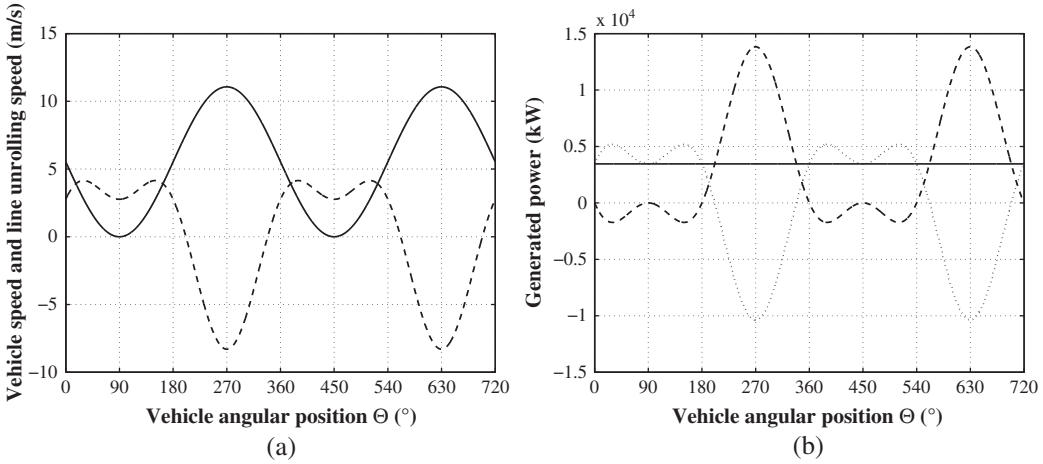

Figure 16. (a) Line speed $\dot{r}$ (dashed) and vehicle speed $R\dot{\Theta}$ (solid) during two complete optimal KE-carousel cycles as functions of Θ. (b) Power P_{vehicle} generated by the vehicle motion (dotted) and power P_{line} given by the line unrolling (dashed) and overall optimal power $P^*_{\text{KE-carousel}}$ (solid).

DOI: 10.1002/rnc

Table IV. Model parameters employed to compute an optimal KE-carousel cycle.

A	500 m^2	Characteristic area
r	600 m	Mean line length
R	300 m	KE-carousel radius
α	12°	Angle of attack ($C_L = 1.3$, $C_D = 0.1$)
d_l	0.04 m	Diameter of a single line
$C_{D,l}$	1	Line drag coefficient
ρ	1.2 kg/m^3	Air density
$\lvert\vec{W}_0\rvert$	8.3 m/s	Nominal wind speed magnitude

position. This would prevent the KE-carousel from completing the cycle; however, such issue could be easily solved by slightly modifying the optimal course of $\dot{\Theta}$, thus tolerating a small performance loss. It has to be noted that although the described results for the KE-carousel with variable cable length are interesting from a theoretical point of view, their practical relevance is moderate, as will be discussed in Section 5.

4. SIMULATION RESULTS

To assess the control system performance and the matching between simplified equations and dynamical model of the system, with the NMPC controllers presented in [11, 25], we performed numerical simulations of the KE-yoyo and of the constant-line KE-carousel. The wind shear profile (Equation (3)) with $Z_{ref} = 32.5$ m, $W_{ref} = 7.4$ m/s, and $Z_r = 6\,10^{-4}$ m (corresponding to the wind profile in Figure 9) has been used during the simulation. Furthermore, to better evaluate the matching between the results obtained through simplified equations and numerical simulation, we performed the latter with no wind disturbances. Simulation results in the presence of wind disturbances can be found in [11, 25].

4.1. KE-yoyo simulation

The model and control parameters employed in the simulation of the KE-yoyo are reported in Table V. The optimal values $\underline{r}^* = 631$ m, $\dot{r}^*_{trac} = 2.14$ m/s, and $\dot{r}^*_{pass} = -6$ m/s computed by

Table V. Numerical simulation of a KE-yoyo with optimized operational cycle: system and control parameters.

m	300 kg	Kite mass
A	500 m^2	Characteristic area
d_l	0.04 m	Diameter of a single line
ρ_l	970 kg/m^3	Line density
$C_{D,l}$	1	Line drag coefficient
α_{trac}	12°	Angle of attack during the traction phase ($C_L = 1.3$, $C_D = 0.1$)
α_{pass}	−6°	Angle of attack during the passive phase ($C_L = 0.02$, $C_D = 0.08$)
ρ	1.2 kg/m^3	Air density
Δr	50 m	Maximum line variation during a cycle
θ_I	55°	Traction phase starting conditions
ϕ_I	45°	
$\underline{r}$	631 m	
$\overline{r}$	681 m	Passive phase starting condition
$\overline{\psi}$	6°	Input constraints
$\overline{\dot{\psi}}$	20°/s	
$\dot{r}_{trac}$	2.14 m/s	Traction phase reference $\dot{r}_{ref}$
$\dot{r}_{pass}$	−6.0 m/s	Passive phase reference $\dot{r}_{ref}$
T_c	0.2 s	Sample time
N_c	1 step	Control horizon
N_p	10 steps	Prediction horizon

DOI: 10.1002/rnc

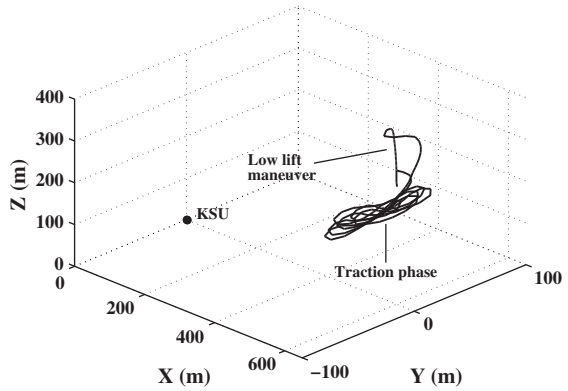

Figure 17. Optimized operation of a KE-yoyo with low-lift maneuver: kite trajectory during one complete cycle simulated using the detailed nonlinear system model and nonlinear model predictive control controller. KSU, Kite Steering Unit.

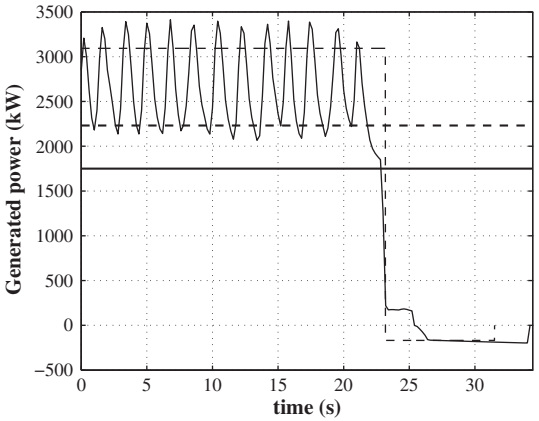

Figure 18. Optimized operation of a KE-yoyo with low-lift maneuver in one complete cycle simulated using the detailed nonlinear system model and nonlinear model predictive control controller. Instantaneous generated power by means of simplified equations (dashed thin line) and by numerical simulation (solid thin line). Average generated power by means of simplified equations (dashed thick line) and by numerical simulation (solid thick line).

solving the optimization problem (28) have been employed as parameters in the numerical simulation. The results related to a complete cycle are presented. The obtained kite trajectory is reported in Figure 17. During the traction phase, the kite follows 'figure eight' orbits, and its elevation Z goes from about 214 to 389 m, corresponding to a mean value of $\theta(t)$ equal to 68°, consistently with the optimized value (29), whereas the lateral angle $\phi(t)$ oscillates between $\pm 10°$ with zero on average. The power generated in the simulation is reported in Figure 18, where it is compared with the optimal power course computed using the simplified equations: the mean simulated value is 1.75 MW, thus showing an error of about 20% with respect to the optimal value (2.2 MW), because of the presence of the inertial and apparent forces, the cable weight and the idle time between the traction and passive phases. In fact, such aspects are not taken into account in the simplified equations.

4.2. KE-carousel simulation with constant cable length

The numerical simulation of the constant-cable KE-carousel has been performed by employing the optimal parameters $r^* = 375$ m and $R\dot{\Theta}^* = 3.98$ m/s according to Equation (36). Furthermore, the system and control parameters used in the simulation are reported in Table VI. The results related to one complete cycle of the KE-carousel are presented. In particular, the obtained kite trajectory

DOI: 10.1002/rnc

Table VI. Numerical simulation of a KE-carousel with optimized operational cycle: system and control parameters.

m	300 kg	Kite mass
A	500 m^2	Characteristic area
R	300 m	KE-carousel radius
d_l	0.04 m	Diameter of a single line
ρ_l	970 kg/m^3	Line density
$C_{\mathrm{D,l}}$	1	Line drag coefficient
α	12°	Angle of attack ($C_\mathrm{L} = 1.3$, $C_\mathrm{D} = 0.1$)
ρ	1.2 kg/m^3	Air density
r	335 m	Line length
$R\dot{\Theta}$	3.9 m/s	Vehicle longitudinal velocity
$\overline{\psi}$	6°	Input constraints
$\overline{\dot{\psi}}$	20°/s	
T_c	0.2 s	Sample time
N_c	1 step	Control horizon
N_p	10 steps	Prediction horizon

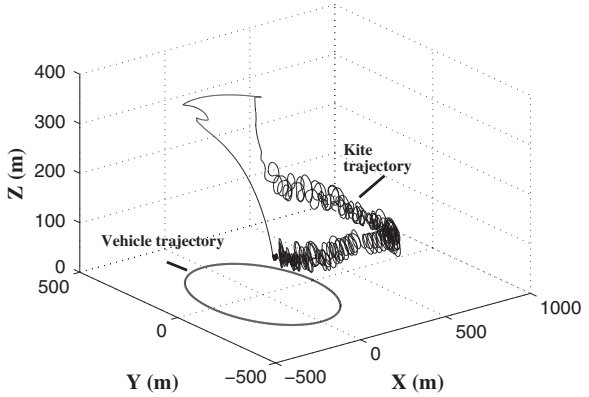

Figure 19. Optimized operation conditions of a KE-carousel with constant cable length. Vehicle and kite trajectories during one complete cycle simulated using the detailed nonlinear system model and nonlinear model predictive control controller.

is shown in Figure 19, and a comparison between the generated power obtained in the simulation and the corresponding optimal result obtained by solving Equation (35) is reported in Figure 20. The mean generated power obtained in the simulation is 1.78 MW, thus showing an error of about 5% with respect to the optimal value (1.89 MW). The courses of the angle $\theta(t)$ and $\phi(t)$, together with the optimal values θ_i^* and ϕ_i^* that solve Equation (35), are reported in Figure 21(a) and 21(b), respectively. It can be noted that the system behavior with the employed controller is very close to the optimal operation.

5. CONCLUSIONS

This paper presented an overview of the innovative Kitenergy technology, which, by exploiting controlled tethered wings to extract energy from high-altitude wind, has the potential to provide large quantities of renewable energy at a lower cost than fossil energy, thus realizing a radical shift in the energy scenario. As a novel contribution with respect to previous works, the operational cycles of Kitenergy generators have been optimized by using simplified power equations in order to evaluate the maximal power that can be generated. Finally, simulations with a detailed system model have been carried out to test the optimized operational cycles and to assess the performance of the employed control strategy on the basis of NMPC. The simulation results showed that the designed

DOI: 10.1002/rnc

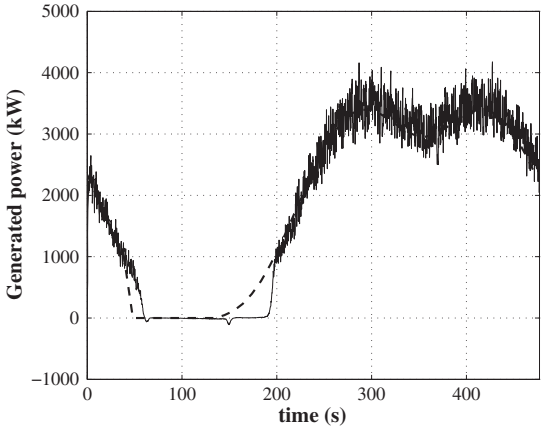

Figure 20. Optimized operation of a constant-cable KE-carousel during one cycle, simulated using the detailed nonlinear system model and nonlinear model predictive control controller. Course of the generated power (solid line) and comparison with the optimized course obtained by using the simplified equations (dashed).

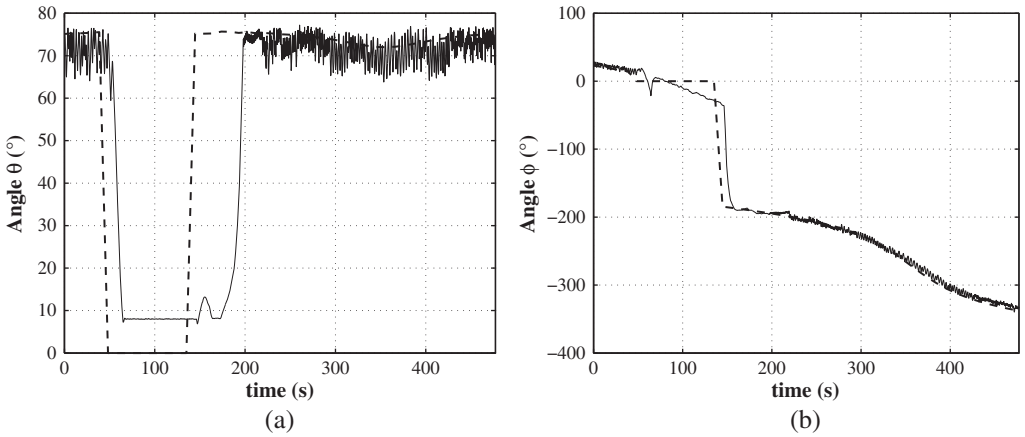

Figure 21. Optimized operation of a constant-cable KE-carousel during one cycle, simulated using the detailed nonlinear system model and nonlinear model predictive control controller. Courses of angle (a) θ and (b) ϕ obtained in the numerical simulation (solid) and by using the simplified equations (dashed).

controller is able to achieve power generation values that are quite close to the ones that have been optimized by using the simplified equations, even if the employed prediction and control horizons are much shorter than the duration of the operating phase, while satisfying operational constraints. Thus, the presented study confirms the results obtained so far regarding the energy generation potentials of Kitenergy technology. Moreover, the reported analyses provide a quite simple and fast way to compute the optimal operating conditions and power output of a Kitenergy generator in a given site. It has to be noted that the employed equations do not take into account the efficiency of energy conversion in the electric drives that convert the mechanical power into electricity, and vice versa: this aspect has to be further investigated in order to improve the estimates of electric energy production/consumption in each operating phase. Finally, the obtained results allow one to carry out a more complete comparison between the different Kitenergy configurations. In particular, with the considered wing and wind characteristics, similar average power values of about 1.8 MW have been obtained with the KE-yoyo and with the constant-cable KE-carousel configurations. It can be noted that the maximal values of the instantaneous generated power in these configurations are about 3.2

DOI: 10.1002/rnc

and 3.3 MW, respectively. Thus, the rated power of the generators equipped on the KSU (for the KE-yoyo) and on the vehicle (for the KE-carousel with constant cable) have to be about 3.2 and 3.3 MW, respectively (i.e., less than twice the mean generated power). These two configurations have similar power generation characteristics but have very different operational cycles, which lead to diverse advantages and potential problems. In fact, being the KSU fixed on the ground, a KE-yoyo is less complex and expensive to build than a constant-cable KE-carousel; however, it may have problems related to excessive cable wear due to line rolling/unrolling under high traction forces. The latter problem is avoided by the KE-carousel with constant cable length. As regards the KE-carousel with variable vehicle speed and cable length, it has been shown in this paper that the maximal overall power can be continuously generated with this configuration without passive phases. In particular, a power of about 3.4 MW has been obtained in the considered conditions, that is, about 60%–80% higher than the average power achieved by the other configurations. However, the rated power of the generators equipped on the vehicle and on the KSU have to be about 15 and 10 MW, respectively, thus requiring an overall rated power that is more than 10 times higher than the average generated power. Thus, the advantages of a higher and a more constant net power generation achieved by the latter configuration are paid in terms of larger costs, for the electric equipments and for the mechanical structure, and of higher construction complexity. These results will be important in the next steps of the research activities, where the trade-off among these different features has to be assessed to select the 'best' configuration to be used for the development of industrial large-scale Kitenergy generators.

APPENDIX

Proof of Proposition 1

The total drag force $\vec{F}_{\mathrm{D,tot}}$ is aligned with the effective wind speed vector $\vec{W}_{\mathrm{e}}$, whereas the lift force $\vec{F}_{\mathrm{L}}$ is perpendicular to $\vec{F}_{\mathrm{D,tot}}$ and, under Assumptions 1–5, it lies on the plane $(\vec{W}_{\mathrm{e,p}}, \vec{e}_r)$. Note that also vectors $\vec{e}_r$ and $\vec{W}_{\mathrm{e,p}}$ are perpendicular, because, by definition, $\vec{W}_{\mathrm{e,p}}$ is the projection of $\vec{W}_{\mathrm{e}}$ on the plane perpendicular to $\vec{e}_r$. Thus, the angle β between $\vec{F}_{\mathrm{D,tot}}$ and $\vec{W}_{\mathrm{e,p}}$ is the same as the angle between vectors $\vec{F}_{\mathrm{L}}$ and $\vec{e}_r$ (Figure 11). Because inertial and apparent forces are negligible, the following equilibrium condition on the plane perpendicular to vector $\vec{e}_r$ has to be satisfied:

$$|\vec{F}_{\mathrm{L}}| \sin(\beta) = |\vec{F}_{\mathrm{D,tot}}| \cos(\beta). \tag{A1}$$

Thus, it can be noted that

$$\frac{|\vec{F}_{\mathrm{D,tot}}|}{|\vec{F}_{\mathrm{L}}|} = \frac{\sin(\beta)}{\cos(\beta)}, \tag{A2}$$

and that, from Equation (18),

$$\frac{\sin(\beta)}{\cos(\beta)} = \frac{C_{\mathrm{D,eq}}}{C_{\mathrm{L}}} = \frac{1}{E_{\mathrm{eq}}}. \tag{A3}$$

□

Proof of Corollary 1

Define the function $f(\beta)$ as

$$f(\beta) \doteq \tan(\beta) - \frac{1}{E_{\mathrm{eq}}} = \tan(\beta) - \frac{1}{C_{\mathrm{L}}}\left(C_{\mathrm{D}} + \frac{2rd_{\mathrm{l}}C_{\mathrm{D,l}}\cos(\beta)}{4A}\right). \tag{A4}$$

Then, Equation (A3) can rewritten as

$$f(\beta) = 0. \tag{A5}$$

DOI: 10.1002/rnc

First, note that $f(\beta)$ is a continuous function in the closed interval $[0; (\pi/2) - \varepsilon]$, where $\varepsilon > 0$ can be eventually arbitrarily small. For $\beta = 0$, $f(\beta) < 0$, in fact,

$$f(0) = -\frac{1}{C_{\mathrm{L}}}\left(C_{\mathrm{D}} + \frac{2rd_{\mathrm{l}}C_{\mathrm{D,l}}}{4A}\right) < 0. \tag{A6}$$

Besides, as $\varepsilon \to 0$, then $f\left((\pi/2) - \varepsilon\right) \to +\infty$. This means that, for ε small enough, then

$$f\left(\frac{\pi}{2} - \varepsilon\right) > 0. \tag{A7}$$

Therefore, because $f(\beta)$ is a continuous function in the interval $[0; (\pi/2) - \varepsilon]$ and Equations (A6)–(A7) hold, from Bolzano's theorem, there exists at least one value of $\beta \in [0; (\pi/2) - \varepsilon]$ satisfying Equation (A5).

To prove that there exists only one value of $\beta \in [0; (\pi/2) - \varepsilon]$ satisfying Equation (A5), we are left to prove that $f(\beta)$ is strictly monotonically increasing in $[0; (\pi/2) - \varepsilon]$. This can be easily proved by considering that both functions $\tan(\beta)$ and

$$-\frac{1}{C_{\mathrm{L}}}\left(C_{\mathrm{D+}}\frac{2rd_{\mathrm{l}}C_{\mathrm{D,l}}\cos(\beta)}{4A}\right)$$

are strictly monotonically increasing over $[0; (\pi/2) - \varepsilon]$. □

Proof of Proposition 2

By considering the trigonometrical relationship $\cos(\beta)^2 + \sin(\beta)^2 = 1$, Equation (A3) leads to

$$\begin{aligned}
\cos(\beta)^2 &= 1 - \sin(\beta)^2 = 1 - \frac{\cos(\beta)^2}{E_{\mathrm{eq}}^2},\\
\cos(\beta)^2\left(1 + \frac{1}{E_{\mathrm{eq}}^2}\right) &= 1,\\
\cos(\beta) &= \sqrt{\frac{E_{\mathrm{eq}}^2}{\left(E_{\mathrm{eq}}^2 + 1\right)}},\\
\sin(\beta) &= \sqrt{\frac{1}{\left(E_{\mathrm{eq}}^2 + 1\right)}}.
\end{aligned} \tag{A8}$$

Now, the traction force $F^{\mathrm{c,trc}}\vec{e}_r$, $F^{\mathrm{c,trc}} \geqslant 0$ acting on the cable, by which mechanical power can be generated, is the sum of the projections of vectors $\vec{F}_{\mathrm{L}}$ and $\vec{F}_{\mathrm{D,tot}}$ on the cable direction $\vec{e}_r$:

$$F^{\mathrm{c,trc}}\vec{e}_r = \vec{F}_{\mathrm{L}} \cdot \vec{e}_r + \vec{F}_{\mathrm{D,tot}} \cdot \vec{e}_r, \tag{A9}$$

whose magnitude in the considered framework can be computed as (Figure 11)

$$F^{\mathrm{c,trc}} = |\vec{F}_{\mathrm{L}}|\cos(\beta) + |\vec{F}_{\mathrm{D,tot}}|\sin(\beta). \tag{A10}$$

Thus, by considering Equations (A8) and (A10), the following equation for the traction force is obtained:

$$F^{\mathrm{c,trc}} = \tfrac{1}{2}\rho A C_{\mathrm{L}}\sqrt{\tfrac{E_{\mathrm{eq}}^2}{(E_{\mathrm{eq}}^2+1)}}|\vec{W}_{\mathrm{e}}|^2 + \tfrac{1}{2}\rho A\tfrac{C_{\mathrm{L}}}{E_{\mathrm{eq}}}\sqrt{\tfrac{1}{(E_{\mathrm{eq}}^2+1)}}|\vec{W}_{\mathrm{e}}|^2. \tag{A11}$$

With straightforward manipulations, Equation (A11) leads to

$$F^{\mathrm{c,trc}} = \tfrac{1}{2}\rho A C_{\mathrm{L}}\sqrt{\tfrac{E_{\mathrm{eq}}^2+1}{E_{\mathrm{eq}}^2}}|\vec{W}_{\mathrm{e}}|^2. \tag{A12}$$

DOI: 10.1002/rnc

Moreover, consider the projection $\vec{W}_{e,r} = \vec{W}_e \cdot \vec{e}_r$ of the effective wind speed on the cable direction. It can be noted that, by construction (Figure 11) and because of Equation (A8), the following relationship holds:

$$|\vec{W}_e| = \frac{|\vec{W}_{e,r}|}{\sin(\beta)} = |\vec{W}_{e,r}| \sqrt{\frac{E_{eq}^2+1}{1}}. \tag{A13}$$

By substituting Equation (A13) in Equation (A12), the following result is obtained:

$$F^{c,trc} = \frac{1}{2}\rho A C_L \sqrt{\frac{E_{eq}^2+1}{E_{eq}^2}} \left(E_{eq}^2+1\right) |\vec{W}_{e,r}|^2,$$

$$F^{c,trc} = \tfrac{1}{2}\rho A C_L E_{eq}^2 \left(1+\tfrac{1}{E_{eq}^2}\right)^{\frac{3}{2}} |\vec{W}_{e,r}|^2 = C|\vec{W}_{e,r}|^2, \tag{A14}$$

with

$$C = \frac{1}{2}\rho A C_L E_{eq}^2 \left(1+\frac{1}{E_{eq}^2}\right)^{\frac{3}{2}}. \tag{A15}$$

□

Proof of Proposition 3

First, it is worth remarking that in the KE-yoyo configuration, the effective wind speed on the cable direction in Equation (23) can be expressed as

$$\vec{W}_{e,r} = |\vec{W}_0(r,\theta)| \sin(\theta)\cos(\phi) - \dot{r}, \tag{A16}$$

because $\Theta = \dot{\Theta} = 0$.

Then, the power $P_{trac}(\tau)$ generated in the traction phase can be written as

$$P_{trac}(\tau) = F_{trac}^{c,trc}(\tau)\dot{r}_{trac}(\tau) = C|\vec{W}_{e,r}|^2 \dot{r}_{trac}(\tau). \tag{A17}$$

Under Assumptions 7 and 9, the angles θ_{trac} and ϕ, as well as the cable length r are approximately constant. Therefore, the effective wind speed $\vec{W}_{e,r}$ (Equation (23)) and the coefficient C (Equation (A16)) assume constant values over the time. Furthermore, under Assumption 8, the cable unrolling speed $\dot{r}_{trac}$ is constant, thus the power $P_{trac}(\tau)$ in Equation (A17) does not depend on the time, then the energy generated during the traction phase can be computed as

$$\int_{t_0}^{t_{trac,end}} P_{trac}(\tau)\,d\tau = \int_{t_0}^{t_{trac,end}} F_{trac}^{c,trc}\dot{r}_{t_{trac}}\,d\tau = F_{trac}^{c,trc}\dot{r}_{trac}\int_{t_0}^{t_{trac,end}} d\tau = F_{trac}^{c,trc}\dot{r}_{trac}\left(t_{trac,end}-t_0\right). \tag{A18}$$

From similar considerations, the energy spent during the passing the passive phase can be approximated as

$$\int_{t_{trac,end}}^{t_{pass,end}} P_{pass}(\tau)\,d\tau \simeq F_{pass}^{c,trc}\dot{r}_{pass}\left(t_{trac,end}-t_{pass,end}\right). \tag{A19}$$

By substituting Equations (A18) and (A19) in Equation (24), it follows that

$$\overline{P} = \frac{\left(F_{trac}^{c,trc}\dot{r}_{trac}(t_{trac,end}-t_0)\right) + \left(F_{pass}^{c,trc}\dot{r}_{pass}(t_{pass,end}-t_{trac,end})\right)}{t_{pass,end}-t_0}. \tag{A20}$$

Note that also Equation (24) could be employed in the following analyses, for example, using numerical integration; however, the increase of accuracy with respect to the simplified equation (A20)

DOI: 10.1002/rnc

would be negligible. Now, by imposing a periodicity condition on the cable length r and considering the fixed cable length variation Δr, the time intervals $(t_{\text{trac,end}} - t_0)$ and $(t_{\text{pass,end}} - t_{\text{trac,end}})$ can be expressed as functions of $\dot{r}_{\text{trac}}$ and $\dot{r}_{\text{pass}}$ as follows (recalling that $\dot{r}_{\text{pass}} < 0$):

$$\begin{aligned}(t_{\text{trac,end}} - t_0) &= \tfrac{\Delta r}{\dot{r}_{\text{trac}}} \\ (t_{\text{pass,end}} - t_{\text{trac,end}}) &= \tfrac{-\Delta r}{\dot{r}_{\text{pass}}}.\end{aligned} \tag{A21}$$

On the basis of Equations (A20) and (A21), through straightforward algebraic manipulations, the simplified equation of the average generated power provided by Equation (25) is obtained. □

Proof of Proposition 4
The point $(\theta, \phi, \dot{r})^T$ in Equation (41) is a feasible solution to problem (39) because it satisfies the constraint

$$\dot{r} \leqslant \sin(\theta)\left(|\vec{W}_0|\cos(\Theta + \phi) - R\,\dot{\Theta}\sin(\phi)\right).$$

By substituting the values of $(\theta, \phi, \dot{r})^T$ reported in Equation (41) in the objective function of Equation (39), the following result is obtained:

$$P^{\text{var}}_{\text{KE-carousel}}(\Theta, \dot{\Theta}) = \frac{4}{27} C\,|\vec{W}_0|^3 \quad \forall \Theta, \dot{\Theta} \in \mathbb{R}. \tag{A22}$$

On the other hand, in the seminal paper by Loyd [8], it has been proved that the maximum power that can be generated by a tethered wing is always smaller than or equal to $(4/27)C\,|\vec{W}_0|^3$, thus

$$P^{\text{var}}_{\text{KE-carousel}}(\Theta, \dot{\Theta}) \leqslant \frac{4}{27} C\,|\vec{W}_0|^3 \quad \forall \Theta, \dot{\Theta} \in \mathbb{R}. \tag{A23}$$

From Equations (A22) and (A23), Equation (40) is obtained, and it results that $(\theta^*, \phi^*, \dot{r}^*)^T$ (Equation (41)) is a global optimizer for Equation (39). □

Proof of Proposition 5
When $\dot{\Theta} = \frac{2}{3R}|\vec{W}_0|(1 - \sin(\Theta))$, the cable speed $\dot{r} = \dot{r}^*$ is equal to

$$\dot{r}(\Theta) = \dot{r}^*(\Theta) = \tfrac{|\vec{W}_0|}{3} + \tfrac{2}{3}|\vec{W}_0|(1 - \sin(\Theta))\sin(\Theta) = \tfrac{|\vec{W}_0|}{3} + \tfrac{2}{3}|\vec{W}_0|\sin(\Theta) - \tfrac{2}{3}|\vec{W}_0|\sin^2(\Theta). \tag{A24}$$

By integrating both sides of Equation (A24) in the interval $[0,\ 2\pi]$, it is obtained that

$$\begin{aligned}\int_0^{2\pi} (\dot{r}(\Theta))\ \mathrm{d}\Theta &= \int_0^{2\pi} \frac{|\vec{W}_0|}{3}\,\mathrm{d}\Theta + \int_0^{2\pi} \frac{2}{3}|\vec{W}_0|\sin(\Theta)\,\mathrm{d}\Theta - \int_0^{2\pi} \frac{2}{3}|\vec{W}_0|\sin^2(\Theta)\,\mathrm{d}\Theta \\ &= \frac{|\vec{W}_0|}{3}2\pi - \frac{2}{3}|\vec{W}_0|\pi = 0,\end{aligned} \tag{A25}$$

as stated in Equation (43). □

ACKNOWLEDGEMENTS

This research has received funding from Regione Piemonte, Italy, under the Projects 'Controllo di aquiloni di potenza per la generazione eolica di energia', 'KiteGen: generazione eolica di alta quota', and 'KiteNav - Power Kites for Naval Propulsion', and from the European Union Seventh Framework Programme (FP7/2007-2013) under grant agreement number PIOF-GA-2009-252284 - Marie Curie project 'Innovative Control, Identification and Estimation Methodologies for Sustainable Energy Technologies'.

DOI: 10.1002/rnc

REFERENCES

1. Global wind energy council. *Global Wind 2007 Report*, May 2008. (Available from: http://www.gwec.net/fileadmin/documents/test2/gwec-08-update_FINAL.pdf).
2. Archer CL, Jacobson MZ. Evaluation of global wind power. *Journal of Geophysical Research* 2005; **110**:D12110.
3. Masters GM. *Renewable and Efficient Electric Power Systems*. Wiley: New Jersey, 2004.
4. Thresher R, Robinson M, Veers P. To capture the wind. *IEEE Power & Energy Magazine* 2007; **5**(6):34–46.
5. Archer CL, Caldeira K. Global assessment of high-altitude wind power. *Energies* 2009; **2**(2):307–319.
6. Manalis MS. Airborne windmills and communication aerostats. *Journal of Aircraft* 1976; **13**(7):543–544.
7. Fletcher CAJ, Roberts BW. Electricity generation from jet-streams winds. *Journal of Energy* 1979; **3**:241–249.
8. Loyd ML. Crosswind kite power. *Journal of Energy* 1980; **4**(3):106–111.
9. Ilzhöfer A, Houska B, Diehl M. Nonlinear MPC of kites under varying wind conditions for a new class of large-scale wind power generators. *International Journal of Robust and Nonlinear Control* 2007; **17**:1590–1599.
10. Canale M, Fagiano L, Milanese M. Power kites for wind energy generation. *IEEE Control Systems Magazine* 2007; **27**(6):25–38.
11. Canale M, Fagiano L, Milanese M. High altitude wind energy generation using controlled power kites. *IEEE Transactions on Control Systems Technology* 2010; **18**(2):279–293. DOI: 10.1109/TCST.2009.2017933.
12. Fagiano L, Milanese M, Piga D. High-altitude wind power generation. *IEEE Transactions on Energy Conversion* 2010; **25**(1):168–180. DOI: 10.1109/TEC.2009.2032582.
13. Ockels WJ. Laddermill, a novel concept to exploit the energy in the airspace. *Aircraft Design* 2001; **4**(2):81–97.
14. Williams P, Lansdorp B, Ockels W. Optimal crosswind towing and power generation with tethered kites. *Journal of Guidance, Control, and Dynamics* 2008; **31**:81–93.
15. Platzer M, Young J, Lai J. Flapping wing technology: the potential for air vehicle propulsion and airborne power generation. *26th International Congress of the Aeronautical Sciences*, Anchorage, Alaska, 2008.
16. Joby Energy Inc. (Available from: http://www.jobyenergy.com).
17. Magenn Power Inc. (Available from: http://www.magenn.com).
18. Makani Power Inc. (Available from: http://www.makanipower.com).
19. Sky Wind Power Corporation. (Available from: http://www.skywindpower.com).
20. SkyMill Energy Inc. (Available from: http://www.skymillenergy.com).
21. SkySails GmbH & Co. (Available from: http://www.skysails.info).
22. KiteNav project website. (Available from: http://www.kitenav.com).
23. Fagiano L, Milanese M, Razza V, Gerlero I. Offshore high-altitude wind energy using controlled airfoils. *European Wind Energy Conference (EWEC) 2010*, Warsaw, PL, 2010.
24. Vestas Wind Systems A/S. Vestas v90 brochure. (Available from: http://www.vestas.com).
25. Fagiano L. Control of tethered airfoils for high–altitude wind energy generation. *PhD Thesis*, Politecnico di Torino, Italy, February 2009. (Available from: http://lorenzofagiano.altervista.org/docs/PhD_thesis_Fagiano_Final.pdf).
26. National Oceanic & Atmospheric Administration – Earth System Research Laboratory. NOAA/ESRL Radiosonde Database Access. (Available from: http://raob.fsl.noaa.gov/).
27. Mayne DQ, Rawlings JB, Rao CV, Scokaert P. Constrained model predictive control: stability and optimality. *Automatica* 2000; **36**:789–814.
28. International Energy Agency (IEA). *Projected Cost of Generating Energy – 2005 Update*. IEA PUBLICATIONS: Paris, France, 2008. (Available from: http://www.iea.org/Textbase/publications/free_new_Desc.asp?PUBS_ID=1472).
29. Kitenergy project, experimental test movie. January 2008. (Available from: http://lorenzofagiano.altervista.org/movies/Casale_test.wmv).
30. Kitenergy project, experimental test movie. August 2006. (Available from: http://lorenzofagiano.altervista.org/movies/Sardinia_test.wmv).
31. Argatov I, Rautakorpi P, Silvennoinen R. Estimation of the mechanical energy output of the kite wind generator. *Wind Energy* 2009; **34**:1525–1532.

DOI: 10.1002/rnc